An ImageJ macro tool for OCTA-based Quantitative Analysis of Myopic Choroidal Neovascularization

Aadit Deshpande, Sundaresan Raman

Department of Computer Science, Birla Institute of Technology and Science Pilani, India

Abstract

Myopic Choroidal neovascularization (mCNV) is one of the most common vision-threatening complications of pathological myopia. Optical Coherence Tomography Angiography (OCTA) has emerged as a non-invasive imaging technique and is routinely included in clinical studies to monitor mCNV in different stages of treatment. However, there exists no standard tool for time-efficient and dependable analysis of OCTA images of mCNV. This study aims to bridge this gap by proposing a customizable ImageJ macro that automates the OCTA image processing and lets users measure nine mCNV biomarkers. We developed an image processing pipeline that filtered the images using the Mexican Hat function, followed by skeletonization. Vascular parameters like Junction Density, Vessel Diameter, and Fractal Dimension were then computed from the skeletonized images. 26 OCTA images were used to test the macro. Two trends emerged in the measurements, in which lesion-size dependent parameters (like mCNV Area) showed variability, while normalized parameters (like Vessel Density) were uniform throughout the dataset. The computed values were within the range of those measured manually and consistent with existing literature. These test results illustrate the macro to be a convenient and customizable tool for future researchers to simultaneously process numerous OCTA images and obtain a systematic, reliable analysis of mCNV.

Introduction

Myopic Choroidal neovascularization (mCNV) is a type-2 CNV that distorts retinal anatomy and is a significant vision-threatening complication of pathologic myopia **[1 Wang Y]**. A population-based study reported that the mCNV was prevalent in 5-11% of individuals with pathologic myopia **[3 Wong TY]**. Several modalities such as FFA (Fluorescein Angiography), SD-OCT (Spectral Domain Optical Coherence Tomography), and OCTA (Optical Coherence Tomography Angiography) help in the diagnosis of this condition **[4 Bagchi]**.

OCTA is a non-invasive technique used to obtain sensitive images for quantitative analysis to monitor mCNV in different stages of treatment. Cheng et al. **[5]** reported mCNV area and flow area as indicators of the effectiveness of intravitreal therapy with Ranibizumab or Conbercept.

Wang et al. **[1]** developed on this and discussed more OCTA biomarkers, such as fractal dimension, junction density, and concluded vessel junctions to be the most predictive biomarker in patients undergoing anti-VEGF treatment. Li et al. **[2]** found branching to be the most sensitive criterion to determine further treatment. They developed a novel procedure combining OCTA and vascular branching to evaluate neovascular activity in mCNV.

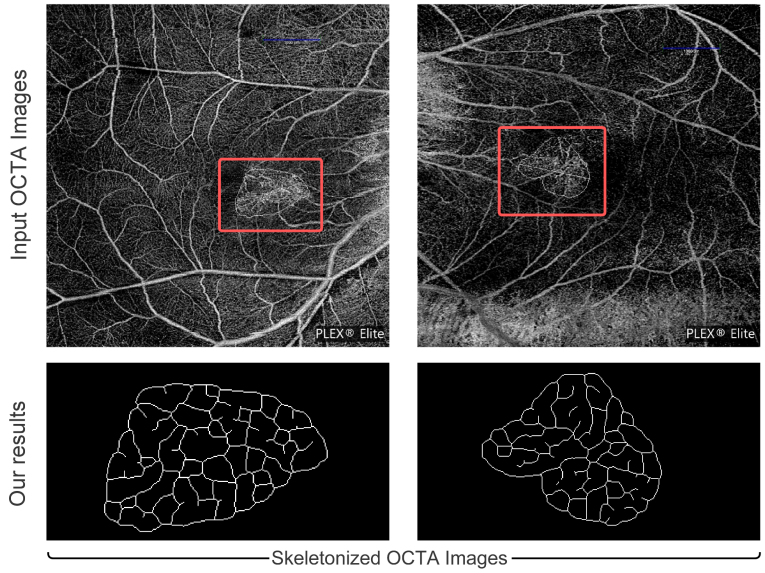

OCTA Biomarkers	*Image 1*	*Image 2*
mCNV area, mm^2	0.837	0.874
Vessel Area, mm^2	0.395	0.410
Vessel Junctions	86.000	69.000
Vessel Length, mm	13.690	13.096
Fractal Dimension	1.377	1.354
Tortuosity	1.100	1.116
Vessel Density	0.472	0.468
Junction Density, n/mm	6.282	5.269
Vessel Dimaeter, µm	28.824	31.272

Fig. 1 Skeletonization and Quantitative Analysis of OCTA images. *We present an ImageJ macro that processes OCTA images of mCNV (Myopic Choroidal neovascularization). Our work enables users to perform quantitative analysis on skeletonized images of active mCNV lesions using nine computed biomarkers.*

All the studies mentioned above developed their own custom programs to process the OCTA images. Software such as MATLAB and ImageJ (Fiji) were commonly used for image processing. Although these have been effective in measuring the biomarkers, there seems to exist no standard tool to aid in the quantitative analysis of OCTA images of mCNV. We aim to fill in this gap by developing an ImageJ macro for the exact purpose of measuring biomarkers from manually segmented OCTA images obtained by commercial SD-OCT systems.

In the present study, we have created an ImageJ macro that allows users to measure nine mCNV parameters from OCTA images. We built upon the algorithm proposed by Wang et al.**[1]**, for mCNV image processing, and applied the Mexican Hat Filter before skeletonization**.** This modified process grants users finer control over the image processing parameters. The macro presents the extracted parameters for a batch of preprocessed OCTA images in tabular form. It also allows users to save intermediate stages of the mCNV images for further analysis.

In this paper, we first discuss the acquisition of OCTA images from patients with mCNV. Then we describe the nine parameters we plan to measure, also detailing the respective image

processing techniques chosen. Next, we show a demonstration of the plugin on a sample OCTA image and discuss the various stages of the pipeline. Finally, we conclude with a discussion of the results, limitations of this study, and future research paths.

Materials and Methods

OCTA Image Acquisition

During the development phase, we tested the macro on a dataset of 26 expert-labeled OCTA images obtained through a research collaboration with Shankar Nethralaya, Chennai, India. The OCTA images had a resolution of 1024x1024, at a scale of 170 pixels/mm, and were collected from patients with mCNV in different stages of treatment.

Quantitative Evaluation of mCNV Images

We wrote our macro script to process and analyze batches of OCTA images in the ImageJ 1.x Macro language **[6]**. ImageJ is a powerful Java-based image processing program developed by the National Institute of Health, USA. It is specifically designed for image analysis tasks in biological sciences, as described in the existing literature. Using ImageJ analysis tools, the macro we developed measures the following nine OCTA metrics:

1. mCNV Area (mm^2): A lesion size biomarker that indicates the total size of the active mCNV lesion.
2. Vessel Area (mm^2): A vessel size biomarker that indicates the size of the vessel components with flow signals in the lesion.
3. Vessel Density: A vascular biomarker defined as the ratio of the area occupied by vessels to the entire mCNV lesion area.
4. Vessel Length (mm): A vascular biomarker that indicates the total neovascular length of the CNV lesion.
5. Vessel Diameter (μm): A vascular biomarker that indicates the average vessel caliber of the mCNV.
6. Vessel Junctions: A vascular biomarker defined as the number of points of vascular connection, indicating internal branching in the mCNV network.
7. Junction Density (n/mm): A biomarker, defined as the ratio of the number of junctions to the total neovascular length, indicating branching complexity.
8. Fractal Dimension: A biomarker that represents the complexity and the space-filling capacity of the vessel branching pattern.
9. Vessel Tortuosity: A morphologic biomarker that quantifies the microtortuosity of the CNV. Smaller values indicate ‘straighter’ vessels.

Method Overview

The macro uses expert-labeled retinal OCTA images as the input. We use an algorithm based on one proposed by Wang et al. **[1]**. The OCTA images must first be preprocessed by manual

delineation. The pipeline follows a branched structure (Figure 1). In the first branch, a Gaussian Blur filter is used to denoise the images. This is followed by a Hessian-based Frangi filter to detect vessels. Finally, a binary image is obtained using Auto Local Median Thresholding. At this stage, the values of Vessel Area, mCNV Area, and Vessel Density are calculated. In the second branch, Mexican Hat Filter **[7]** is applied to the delineated OCTA images, followed by Skeletonization. The skeletonized image is used to calculate the values of Vessel Length, Junctions, Fractal Dimension and Torutosity. Vessel Diameter and Junction density are derived from the previously calculated parameters.

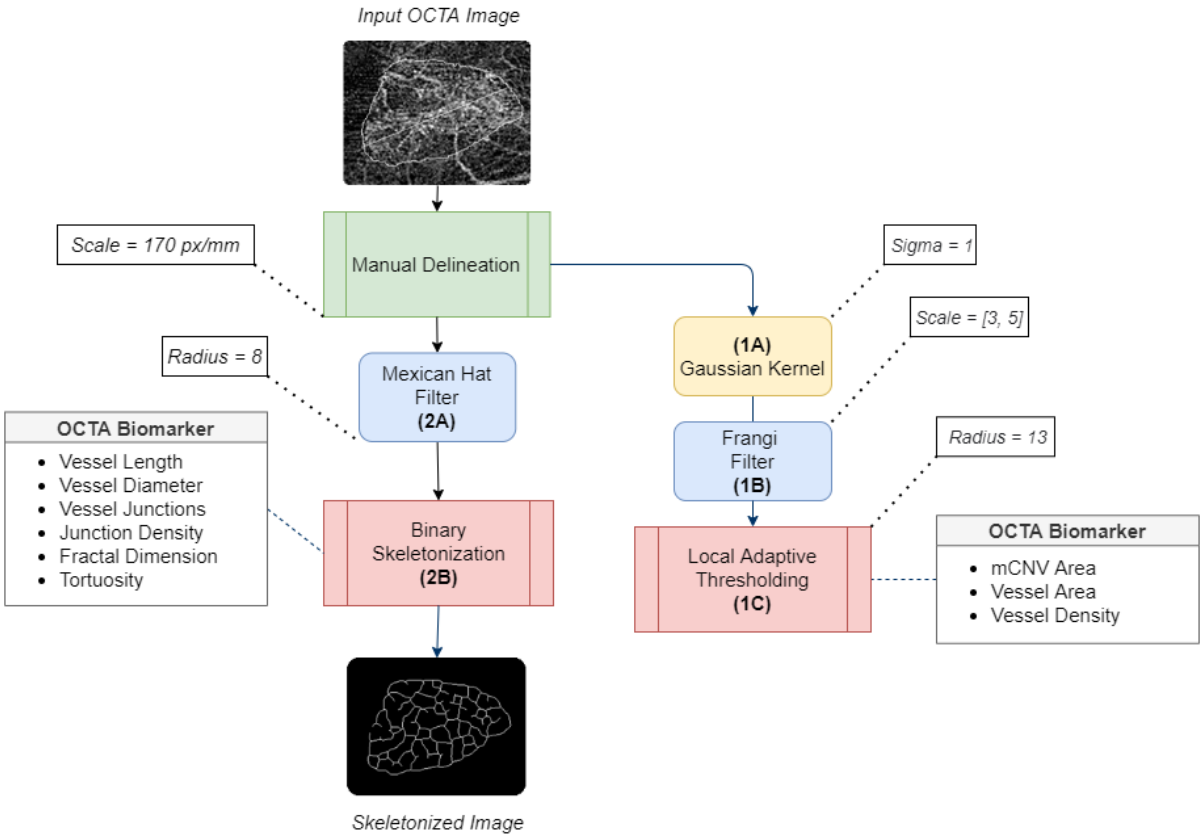

Fig. 2 Pipeline Diagram for processing OCTA images with all stages identified. *Our algorithm takes manually cropped OCTA images as input. The pipeline follows a branched structure. In Branch 1, we denoise the image* ***(1A)****, apply the Frangi filter* ***(1B)****, and use Median Thresholding* ***(1C)*** *to measure area-related biomarkers. In Branch 2, we apply the Mexican Hat filter* ***(2A)*** *and Binary Skeletonization* ***(2B)*** *to measure vascular biomarkers like junctions, diameter, fractal dimension, and tortuosity.*

Overall Pipeline Structure

Fig. 2 shows the overall image processing pipeline of the application. The various stages are detailed below.

Preprocessing

Before entering the pipeline, the expert-labeled OCTA images must be manually delineated to ensure that the vessel biomarkers are measured only in the active mCNV lesion. The cropped images are converted to 8-bit grayscale as a precondition for the Skeletonization stage (2C) further down the pipeline. The mCNV lesion area is measured from the cropped OCTA image.

Gaussian Kernel (1A)

The cropped images are denoised using a Gaussian Blur filter with a radius of decay as 1. This filter uses convolution with a Gaussian function **[8]** for smoothing. The quality of single OCTA images of mCNV is poorer than averaged images, so denoising is beneficial **[17]** for the Frangi filter stage (1B).

$$G(x,y) = \frac{1}{2\pi\sigma^2} e^{-\frac{x^2+y^2}{2\sigma^2}}$$

Hessian Frangi Filter (1B)

The denoised images are passed through a Hessian-based Frangi vesselness filter (*using the ImageJ Frangi plugin **[13]***). This filter uses the eigenvectors of the Hessian to compute the likeliness of the 2D image to contain vessels (Frangi et al. **[9]**). The Frangi vesselness filter is crucial for the Thresholding stage (1C).

Auto Local Thresholding (1C)

The 8-bit images are binarized through local adaptive thresholding *(using the ImageJ Auto Local Threshold plugin **[14]**)*. 'Local' here means that the threshold is computed for each pixel within a window of a certain radius (= 8) around it. The Median method selects the threshold as the median of the local greyscale distribution. The median method was consistently produced better segmentation results than other methods such as the Otsu algorithm **[10]**. The area statistics of the binary image are used to find the Vessel Area. The Vessel Density biomarker is calculated using the values of Vessel Area and mCNV Area.

Mexican Hat Filter (2A)

This branch of the pipeline is used to produce skeletonized binary OCTA images. The cropped images are passed through the Mexican hat Filter *(Mexican hat filter plugin **[12]**)*. The filter is applied over a neighborhood of radius 13 for each pixel (radius value found empirically). This filter uses convolution with the Ricker wavelet function and has proven to be effective for feature detection **[7]**. The Mexican Hat Filter stage is the precursor to Skeletonization.

$$\psi(x,y) = \frac{1}{\pi\sigma^4}\left(1 - \frac{1}{2}\left(\frac{x^2+y^2}{\sigma^2}\right)\right)e^{-\frac{x^2+y^2}{2\sigma^2}}$$

Binary Skeletonization (2B)

Finally, The 8-bit OCTA images are skeletonized (internally implemented using the Binary Thinning Algorithm (Homann et al. **[11]**)). The skeletonized images provide great insight into the vascular activity of the mCNV lesion. The 'AnalyzeSkeleton' ImageJ plugin **[15]** provides a detailed statistical analysis of the branching structure and is used to calculate the Vessel Length, Tortuosity, and number of Junctions. Ratios such as Junction Density and Vessel Diameter are computed using the skeletonized image as well. The vessel complexity is quantified using Fractal Dimension, which is measured by the box-counting method. At this stage, all nine biomarkers have been established.

$$\dim_{\text{box}}(S) = n - \lim_{r \to 0} \frac{\log \text{vol}(S_r)}{\log r},$$

Fig. 3 shows all the intermediate pipeline stages on a sample OCTA image, starting with the input image and ending with the tagged skeleton.

Program Use

The macro can be launched in Fiji without installation. Once the macro is downloaded, it can be opened by selecting the Plugins->Macro->Run option or by simply dragging and dropping the script onto an active ImageJ window. The following choices are offered to the user, on launching the script.

Type of Analysis: The user can input the number of images they want to analyze. A checkbox enables the user to save all the intermediate image processing steps. The user can choose the input image file format, which is set to TIFF by default. The user also selects the target input and output folders for the input images, the output CSV file, and the intermediate pipeline stages.
Input Images: It is highly recommended that the input OCTA images be manually delineated in ImageJ, to achieve accurate results. This can be achieved using any of ImageJ's in-built selection tools, such as Polygon, Freehand, etc., followed by clearing the image area outside the selection.

Customizable Parameters: The user can then adjust the values of parameters in various pipeline stages. The sigma of the Gaussian used in stage 1A can be adjusted depending on the amount of denoising needed. The user can also set the pixel radii for the Local Adaptive Thresholding in Stage 1C and the Mexican Hat filter in Stage 2A, based on the mCNV lesion in the input images. Finally, the user can set the pixel scale (per 1000 μm) for all the subsequent measurements.

Once the script processes the entire batch, a CSV file containing the computed values of all 9 OCTA biomarkers is saved in the output directory. Additionally, if the user checks the “Save Pipeline Stages?” checkbox, the intermediate images (5 per input image) are stored in the specified output directory.

System Requirements: The software requirements are the same as those of Fiji(Image, currently supported on:

- Windows XP, Vista, 7, 8 and 10
- Mac OS X 10.8 “Mountain Lion” or later
- Linux on amd64 and x86 architectures

However, the availability of Java 8 runtime is the only software prerequisite.

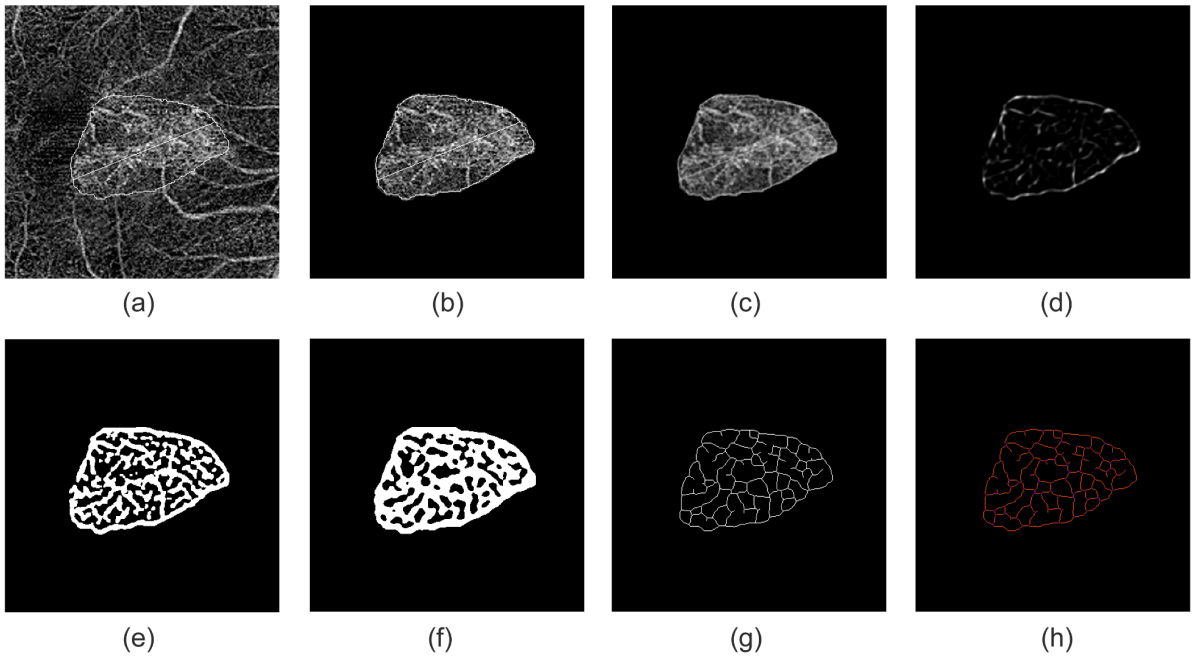

Fig. 3 Intermediate stages of the OCTA image as it travels down the pipeline. (a) *Input OCTA image showing the active mCNV lesion.* ***(b)*** *Manually delineated OCTA image. mCNV area is measured by counting the pixels within the contour.* ***(c)*** *The Gaussian kernel was used for smoothing and denoising the image.* ***(d), (e)*** *The Frangi vesselness filter and Median Thresholding were used to calculate Vessel Area and Vessel Density.* ***(f)*** *The Mexican Hat filter was applied to the cropped image (b).* ***(g)*** *Binary skeletonization of the OCTA image using ImageJ.* ***(h)*** *The tagged skeleton was used to calculate the Junctions, Vessel Diameter, Tortuosity, and Fractal Dimension.*

Table 2 *Statistical Analysis of OCTA biomarkers on the 26 image dataset*

OCTA Biomarkers	*Mean*	*Std. Dev.*	*Min*	*Max*
mCNV area, mm^2	0.649	0.463	0.156	1.951
Vessel Area, mm^2	0.306	0.201	0.078	0.858
Vessel Junctions	59.885	42.813	10	183
Vessel Length, mm	10.238	6.773	2.616	29.315
Fractal Dimension	1.342	0.049	1.194	1.407
Tortuosity	1.124	0.021	1.1	1.188
Vessel Density	0.485	0.021	0.44	0.514
Junction Density, n/mm	5.644	0.635	3.823	6.583
Vessel Dimaeter, µm	30.016	1.415	28.151	33.563

Table 3 *Comparison of our results with those of Yang et al. [1] (Similar study)*

OCTA Biomarkers	*Mean (Our Results)*	*Mean (Similar Study)*	*Std. Dev. (Our Results)*	*Std. Dev. (Similar Study)*
mCNV area, mm^2	0.65	0.40	0.46	0.52
Vessel Area, mm^2	0.31	0.20	0.20	0.20
Vessel Junctions	59.88	49.36	42.81	47.43
Vessel Length, mm	10.24	6.96	6.77	7.92
Fractal Dimension	1.34	1.08	0.05	0.15
Tortuosity	1.12	1.26	0.02	0.07
Vessel Density	0.49	0.55	0.02	0.09
Junction Density, n/mm	5.64	7.52	0.63	1.65
Vessel Dimaeter, µm	30.02	31.11	1.41	3.78

Results

The primary purpose of the macro is to perform quantitative analysis on OCTA images of mCNV and obtain reliable measurements of nine biomarkers. We tested the macro on a dataset of 26 manually-cropped expert-labeled OCTA images (courtesy of Shankar Nethralaya, Chennai, India).

In our results *(Table 2)*, we observed that parameters like mCNV Area (0.65+- 0.40 mm^2), Vessel Area (0.31+-0.20 mm^2), Vessel Junctions(59.88+-49.36), and Vessel Length (10.24+-6.96 mm) had high standard deviation in comparison to their mean values, which indicates a large amount of variation across different images. On the other hand, metrics such as Tortuosity (1.12+-0.02), Fractal Dimension (1.34+-0.05), Vessel Diameter (30.02 +- 1.41 µm), Junction Density (5.64+-0.63 n/mm^2), and Vessel Density (0.49+-0.02) had low standard deviation, indicating that values were clustered around the central value.

We compared the reliability of our results against a similar analysis by Wang et al.[1] (dataset of 31 OCTA images). The statistical analysis for both studies is shown in Table 3. Our measurements for most parameters were consistent with those in existing literature *(Table 3)*. Any differences in the mean or standard deviation were likely due to variation in the datasets. The nine OCTA biomarkers computed by the macro were within the range of expected values obtained manually.

Discussion

The measurements of OCTA biomarkers obtained with the macro are valid, as they're within the range of expected values obtained manually. The trends that emerged in the biomarkers measured in the present study were: (1) High Standard deviation in mCNV Area, Vessel Area, Vessel Junctions, and Vessel Length; (2) Low Standard deviation in Tortuosity, Fractal Dimension, Vessel Diameter, Junction Density, and Vessel Density. The high standard deviation in the values of the former parameters can be explained by the fact that they are lesion-size dependent and that the dataset contained differently sized mCNV lesions, ranging from 0.156 mm^2 (14 junctions) to 1.951 mm^2 (183 junctions). Conversely, the low variation in parameters like Vessel Density and Junction Density can be attributed to them being normalized metrics, making them size-independent. Similarly, Tortuosity and Fractal Dimension have low standard deviations due to the similarities in vascular branching patterns across the OCTA images.

These results are consistent with several related studies. Li et al. **[2]** also observed high variability in the mCNV area (0.62+-0.58 mm^2) in their study on a dataset of 41 eyes with mCNV. Among the parameters with low variability, Mao JB et al. **[19]** reported deep vessel density as 46.21+-5.17%, remarkably similar to our value of 48.5+-2.1%. Similarly, Yao X et al.**[18]** reported a mean difference of -1.3 μm for vessels <45 μm in OCTA scans. Our values of vessel diameter (30.02 +- 1.41 μm) substantiate this result too.

However, we must note the limitations of this study. Firstly, the number of OCTA images in our dataset was relatively small (26 images). This could be a reason why some biomarkers like Tortuosity and Fractal Dimension showed minimal variation and were nearly constant across all 26 images. Secondly, manual delineation of the mCNV area is imperative for accurate measurements from the macro. This may limit the scalability of the macro and its use on a larger batch of images. Finally, the accuracy of the biomarker measurements may be compromised due to artifacts in the skeletonized images. These artifacts are likely due to the CNV boundaries present in the input OCTA images (annotated by experts).

Our results are promising and provide researchers with a customizable, efficient, and reliable method to perform quantitative analysis on OCTA images of mCNV. This opens up an exciting new avenue of study focused on image processing techniques to analyze retinal images. Future work in this domain could take a number of research paths, exploring different thresholding techniques, measuring even more OCTA biomarkers, or using other methods such as the Haursdoff Method to compute parameters like the Fractal Dimension of mCNV.

Conclusion

Pathological myopia is one of the leading causes of blindness, and it is important to understand and quantitatively profile mCNV, a condition found in 5-11% of such individuals. By analyzing OCTA images of mCNV, we propose a standard tool for quantitative analysis that measures nine biomarkers. Following a semi-automated approach, we developed an image processing pipeline that processes a batch of OCTA images to obtain skeletonized images of the mCNV lesion for complete quantitative analysis. We tested the macro on a dataset of 26 OCTA images and observed that parameters like mCNV Area showed much variation, while others like Tortuosity and Vessel Density were uniform throughout. Our results were in the expected range when measured manually and consistent with those of similar studies. Future research into mCNV analysis should focus on improving the accuracy of such automated measurements to remove any potential biases resulting from automation. Furthermore, other new parameters could be measured using different techniques, such as the Haursdoff Method for Fractal Dimension.

References

1. Wang Y, Hu Z, Zhu T, Su Z, Fang X, Lin J, et al. Optical Coherence Tomography Angiography-Based Quantitative Assessment of Morphologic Changes in Active Myopic Choroidal Neovascularization During Anti-vascular Endothelial Growth Factor Therapy. Frontiers in Medicine. 2021;8:586.

2. Wong TY, Ferreira A, Hughes R, Carter G, Mitchell P. Epidemiology and disease burden of pathologic myopia and myopic choroidal neovascularization: an evidence-based systematic review. American journal of ophthalmology. 2014;157(1):9–25.

3. Bagchi A, Schwartz R, Hykin P, Sivaprasad S. Diagnostic algorithm utilising multimodal imaging including optical coherence tomography angiography for the detection of myopic choroidal neovascularisation. Eye. 2019;33(7):1111–1118.

4. Cheng Y, Li Y, Huang X, Qu Y. Application of optical coherence tomography angiography to assess anti-vascular endothelial growth factor therapy in myopic choroidal neovascularization. Retina. 2019;39(4):712–718.

5. Li S, Sun L, Zhao X, Huang S, Luo X, Zhang A, et al. Assessing the activity of myopic choroidal neovascularization: comparison between optical coherence tomography angiography and dye angiography. Retina (Philadelphia, Pa). 2020;40(9):1757.

6. Schindelin J, Arganda-Carreras I, Frise E, Kaynig V, Longair M, Pietzsch T, et al. Fiji: an open-source platform for biological-image analysis. Nature methods. 2012;9(7):676–682.

7. Jin F, Feng D. Image registration algorithm using Mexican hat function-based operator and grouped feature matching strategy. PloS one. 2014;9(4):e95576.

8. Nixon M, Aguado A. Feature extraction and image processing for computer

vision. Academic Press; 2019.

9. Sawai Y, Miyata M, Uji A, Ooto S, Tamura H, Ueda-Arakawa N, et al. Usefulness of Denoising process to Depict Myopic choroidal neovascularisation Using a Single optical coherence tomography Angiography image. Scientific reports. 2020;10(1):1–6.

10. Curtis Rueden ML. Frangi Vesselness Filter-ImageJ [Internet]; [cited 2021 Nov 20]. Available from: https://imagej.net/plugins/frangi.

11. Frangi AF, Niessen WJ, Vincken KL, Viergever MA. Multiscale vessel enhancement filtering. In: International conference on medical image computing and computer-assisted intervention. Springer; 1998. p. 130–137.

12. Landini G. Auto Local Threshold-ImageJ [Internet]; [cited 2021 Nov 20]. Available from: https://imagej.net/plugins/auto-local-threshold.

13. Yang X, Shen X, Long J, Chen H. An improved median-based Otsu image thresholding algorithm. Aasri Procedia. 2012;3:468–473.

14. Prodanov D. Mexican Hat Filter-ImageJ [Internet]; [cited 2021 Nov 20]. Available from: https://imagej.nih.gov/ij/plugins/mexican-hat/index.html.

15. Lee TC, Kashyap RL, Chu CN. Building skeleton models via 3-D medial surface axis thinning algorithms. CVGIP: Graphical Models and Image Processing. 1994;56(6):462–478.

16. Arganda-Carreras I. AnalyzeSkeleton-ImageJ [Internet]; [cited 2021 Nov 20]. Available from: https://imagej.net/plugins/analyze-skeleton/.

17. Mao JB, Shao YR, Yu JF, Deng XY, Liu CY, Chen YQ, et al. Macular density alterations in myopic choroidal neovascularization and the effect of anti-VEGF on it. International Journal of Ophthalmology. 2021;14(8):1205.

18. Yao X, Ke M, Ho Y, Lin E, Wong DW, Tan B, et al. Comparison of retinal vessel diameter measurements from swept-source OCT angiography and adaptive optics ophthalmoscope. British Journal of Ophthalmology. 2021;105(3):426–431.